Research article

Biofunctionalization of titanium surfaces with alendronate and albumin modulates osteoblast performance

Carolina Simão Albano [a,b], Anderson Moreira Gomes [a], Geórgia da Silva Feltran [a],
Célio Junior da Costa Fernandes [a], Luciana Daniele Trino [b], Willian Fernando Zambuzzi [a,1],
Paulo Noronha Lisboa-Filho [b,*,1]

[a] Bioassays and Cell Dynamics Laboratory – UNESP – São Paulo State University, Biosciences Institute, Department of Chemistry and Biochemistry, Botucatu, Brazil
[b] Advanced Materials and Nanotechnology Laboratory – UNESP – São Paulo State University School of Sciences, Department of Physics, Bauru, Brazil

A B S T R A C T

Background: Biofunctionalization of titanium surfaces can improve host responses, especially considering the time for osteointegration and patient recovery. This prompted us to modify titanium surfaces with alendronate and albumin and to investigate the behavior of osteoblasts on these surfaces.
Methods: The biofunctionalization of titanium surfaces was characterized using classical physicochemical approaches and later used to challenge pre-osteoblast cells up to 24 h. Then their viability and molecular behavior were investigated using mitochondrial dehydrogenase activity and RTq-PCR technologies, respectively. Potential stimulus of extracellular remodeling was also investigated by zymography.
Results: Our data indicates a differential behavior of cells responding to the surfaces, considering the activity of mitochondrial dehydrogenases. Molecularly, the differential expression of genes related with cell adhesion highlighted the importance of *Integrin-β1*, *Fak,* and *Src*. These 3 genes were significantly decreased in response to titanium surfaces modified with alendronate, but this behavior was reverted when alendronate was associated with albumin. Alendronate-modified surfaces promoted a significant increase on ECM remodeling, as well as culminating with greater gene activity related to the osteogenic phenotype (*Runx2, Alp, Bsp*).
Conclusion: Altogether, our study found interesting osteogenic behavior of cells in response to alendronate and albumin surfaces, which indicates the need for *in vivo* analyses to better consider these surfaces before clinical trials within the biomedical field.

1. Introduction

Biomaterials play key roles in procedures within the engineering and medicine fields, in which their primary role worldwide is to benefit people's quality of lives with several applications in the dental, orthopedic, and cardiovascular areas [1]. Metal-based alloys are commonly used as biomaterials, especially for implants, and titanium is one of the metals most employed for these purposes. Commercially pure titanium (cp-Ti) and its alloys are promising metals for these biomaterials, due to relevant characteristics that determine the efficacy of the implant, such as biocompatibility and high resistance to corrosion [2, 3], as well as greater interaction with biological tissues than other metals [4, 5, 6, 7, 8, 9, 10].

Although titanium presents considerable interesting and already known properties, improving their biological properties and modifying their surfaces are a very interesting strategy. The surface of the biomaterial is responsible for a significant role with direct contact on the host tissue that ensures the osseointegration of the implant. The interaction with the peri-implant in the early steps of tissue healing determine the success of later stages as appositional tissue growth. Several modifications on the surfaces of the implants have been proposed to improve the interaction between the implant and host tissue [1, 11, 12].

The surface of the titanium is composed of a layer of oxide (TiO₂) that forms promptly. This film is thin and unstable and may not withstand the mechanical stresses required for an implant. Therefore, this native layer must be thickened, since the properties of the film are a decisive factor

* Corresponding author.
  E-mail address: paulo.lisboa@unesp.br (P.N. Lisboa-Filho).
[1] These authors share senior authorship.

that define the degree of corrosion for metal or alloys [13, 14]. In addition to surface treatments to increase TiO_2 film thickness, the literature reports the efficiency of this layer in delivering and releasing specific drugs to optimize the osseointegration process [15, 16, 17, 18]. Several categories of drugs are used for this purpose, but currently attention is focused on the class of bisphosphonates to modulate bone response, by directly hampering the action of osteoclasts [15, 19]. Sodium alendronate is an important drug of interest because of studies that report increased bone density and formation, once it has been used for bone disorders such as osteoporosis [20, 21].

The reactional tissue close to the implant is important for circulating protein for bioactivity of implants, because the biological fluids containing proteins make first contact with the biomaterials, establishing a "biological cap", which will be recognized later by the host cells [22, 23]. Among the circulating proteins with already known properties, albumin (BSA) has important and interesting roles especially considering bloodstream and osteoblast performance [24, 25].

This situation prompted us to evaluate the activity of pre-osteoblastic cells (MC3T3-E1, subclone 4) on the three proposed titanium surfaces, considering TiO_2 thin film, bisphosphonate (alendronate) and albumin (BSA) coatings. Although some studies have look at these materials, further information is needed about the biological performance of osteoblast when in contacting with those surfaces. Better understanding about the biocompatibility and performance of new surfaces are important preclinical issues.

2. Materials and methods

2.1. TiO_2 synthesis and surface modification methodology

Titanium dioxide synthesis. The titanium dioxide solution was synthesized using a sol-gel process, as previously reported by our group [26].

Substrate preparation. Commercial pure titanium discs (12.7 mm diameter and 3 mm thickness) were used as substrates. they were polished (meshes of 320, 400, 600, and 800) to make the surface uniform and to remove the natural oxide layer. The substrates were washed in an ultrasonic bath for 30 min, of which 10 min were immersed in deionized water, 10 min in isopropyl alcohol, and 10 min in deionized water. Then, the samples were hydroxylated in a mixture of 7:3 (v/v) 98% H_2SO_4 and 30% H_2O_2 for 2 h [26].

Oxide deposition. The deposition was performed by the spin coating technique (2000 rpm for 60 s) and this procedure was repeated three times for each sample to acquire thicker layers. Between the depositions, the samples were heated to 40 °C for 5 min. After that, the substrates coated with TiO_2 oxide were annealed at 850 °C for 2 h with a heating rate of 1 °C min^{-1} to obtain a rutile crystalline polymorphic phase [26].

2.2. Deposition of the biomolecules

After growing TiO_2 film on the surfaces, the samples were functionalized with sodium alendronate and albumin, separately. The functionalization of the discs occurred using an immersion method, as described in detail below.

Sodium alendronate. The samples were immersed in a solution containing deionized water and methanol at a 60:40 ratio, respectively. The sodium alendronate (99.99%, Sigma-Aldrich Corp., St. Louis, MO, USA) was then dissolved in the solution at a concentration of 0.5 mg/ml. Three titanium devices remained immersed in 5 ml of the solution for 12 h to maintain control of the samples. Then, the samples were washed with deionized water and heated to 100 °C for 2 h [27].

Albumin (BSA). The samples were immersed in a solution containing 0.4 mg/ml of albumin (BSA, 96%, Sigma-Aldrich Corp., St. Louis, MO, USA) in a phosphate buffer solution (PBS, Sigma-Aldrich Corp.). Three substrates remained immersed in 30 ml of the solution for 6 h to maintain control of the samples. Finally, the samples were washed with PBS and deionized water [28].

TiO_2 surfaces modified with enriched medium. The TiO_2 discs (n = 3) were conditioned in α-MEM medium without FBS up to 24 h at 37 °C, 5% CO_2, and 95% humidity (ISO 10993:2016). This conditioned media contains molecules potentially released by the surfaces.

2.3. TiO_2 surface characterization

The crystal structure of the TiO_2 films was analyzed by X-ray diffraction (XRD, D/MAX-2100/PC, Rigaku) using Cu Kα radiation (λ = 1.54056 Å) coupled to a nickel filter, to eliminate the Cu Kβ radiation. The measurements were taken from 20° to 45°, with regular step of 0.02° min^{-1} and scan speed of 2° min^{-1}, at 40 kV/20 mA. For phase identification, the PCPDF 65–3411, 44–1294, and 76–1949 cards were employed for Ti and TiO_2, respectively.

The XPS measurements were performed on a Kratos spectrometer (AXIS-165) using a monochromatic Al Kα X-ray source. Each sample was analyzed at a 54.7° angle, which is defined as the emission angle relative to the surface. The energy resolution was 0.45 eV. The pass spectrum energy of the spectra was 80 eV and the individual high-resolution spectra was 20 eV. To correct for any charging effect, the binding energy of the Ti $2p^3/_2$ peak was normalized to 458.8 eV. The CasaXPS computational package was used for the chemical study and analysis of the functionalized sample surfaces.

Surface roughness characterization was performed by Confocal Microscopy (Leica DCM3D) employing a 20x lens. Arithmetical surface roughness values (Ra) were determined by calculating the mean value from six randomly selected areas of each sample [29].

2.4. Biological analysis

Osteoblasts and culture conditions. MC3T3-E1 cells (pre-osteoblast cells, subclone 4) were cultured in α minimum essential medium (α-MEM) supplemented with 10% fetal bovine serum (FBS) and 1% antibiotics (penicillin and streptomycin) (NUTRICELL, Campinas, SP, Brazil) and maintained at 37 °C, 5% CO_2, and 95% humidity. In all experiments, trypsinization of the cells was performed in the sub-confluent stage and with low passages (<20).

Cell viability assay. The pre-osteoblasts used were treated with the conditioned medium by the different surfaces modified during the 24-hour period, which were then trypsinized and seeded (1×10^4 cells/ml) into 96-well microplates. The viable cells were stained with the vital dye MTT (1 mg/ml). The insoluble blue dye that formed was resuspended appropriately in dimethylsulfoxide (DMSO) and the cell viability was estimated by measuring absorbance in a microplate reader (SYNERGY-HTX multi-mode reader, Biotek, USA) [30] at a 570 nm wavelength.

Cell adhesion assay. The cells were treated with the conditioned medium for 24 h, then they were trypsinized and seeded (1×10^4 cells/ml) in to 96-well microplates. After 24 h of seeding, cell adhesion was estimated by incorporating the crystal violet. The resulting absorbance was measured at 540 nm using a microplate reader (SYNERGY-HTX, multi-mode reader, Biotek, USA).

Extracellular remodeling stimulus was measured by matrix metalloproteinase activities. Once we had demonstrated the importance of ECM remodeling during the early behavior of osteoblast interacting with biomaterials surfaces, we addressed the proteolytic activities of both Mmp2 and Mmp9 by performing gelatin-based zymography technology. Briefly, the conditioned medium was collected, clarified by centrifugation at 13.200 xg for 15 min at 4 °C and stored at -20 °C. Protein quantification was performed by the Lowry method [31] and the samples were prepared to be applied in equal amounts (150 μg) in 10% (w/v) SDS-polyacrylamide gel and 4% (w/v) gelatin. MMP renaturation was performed in 2% (v/v) Triton X-100 for 40 min, followed by incubation in a proteolysis buffer [50 mM Tris-HCl and 10 mM $CaCl_2$ (pH 7.4)] at 37 °C for 18 h. Subsequently, the gels were stained with 0.5% (w/v) coomassie blue G 250 for 30 min, washed in a 30% (v/v) methanol and 10% (v/v) acetic acid glacial and analyzed using the ImageJ Software [32].

Table 1. Expression primers sequences and PCR cycle conditions.

Gene (ID)	Primer	5′- 3′ Sequence	Reaction Condition
Gene expression			
RUNX2 (12393)	Forward	GGACGAGGCAAGAGTTTCA	95 °C - 15 s; 60 °C - 30 s; 72 °C - 30 s
	Reverse	TGGTGCAGAGTTCAGGGAG	
BSP (103993)	Forward	GTACCGGCCACGCTACTTTCT	95 °C - 15 s; 60 °C - 30 s; 72 °C - 30 s
	Reverse	GTTGACCGCCAGCTCGTTTT	
ALP (11647)	Forward	GAAGTCCGTGGGCATCGT	95 °C - 15 s; 60 °C - 30 s; 72 °C - 30 s
	Reverse	CAGTGCGGTTCCAGACATAG	
MMP9 (17395)	Forward	TGTGCCCTGGAACTCACACGAC	95 °C - 15 s; 60 °C - 30 s; 72 °C - 30 s
	Reverse	ACGTCGTCCACCTGGTTCACCT	
MMP2 (17390)	Forward	AACTTTGAGAAGGATGGCAAGT	95 °C - 15 s; 60 °C - 30 s; 72 °C - 30 s
	Reverse	TGCCACCCATGGTAAACAA	
FAK (14083)	Forward	TCCACCAAAGAAACCACCTC	95 °C - 15 s; 60 °C - 30 s; 72 °C - 30 s
	Reverse	ACGGCTTGACACCCTCATT	
SRC (17977)	Forward	TCGTGAGGGAGAGTGAGAC	95 °C - 15 s; 60 °C - 30 s; 72 °C - 30 s
	Reverse	GCGGGAGGTGATGTAGAAAC	
TIMP2 (21858)	Forward	GCAACAGGCGTTTTGCAATG	95 °C - 15 s; 60 °C - 30 s; 72 °C - 30 s
	Reverse	CGGAATCCACCTCCTTCTCG	
INTEGRIN-B1 (16412)	Forward	CTGATTGGCTGGAGGAATGT	95 °C - 15 s; 60 °C - 30 s; 72 °C - 30 s
	Reverse	TGAGCAATTGAAGGATAATCATAG	
COFILIN (12631)	Forward	CAGACAAGGACTGCCGCTAT	95 °C - 15 s; 60 °C - 30 s; 72 °C - 30 s
	Reverse	TTGCTCTTGAGGGGTGCATT	
PP2A (19052)	Forward	ATGGGCCTCTCTCCCATTCT	95 °C - 15 s; 60 °C - 30 s; 72 °C - 30 s
	Reverse	CATGCACAGGGAGTGACAGT	
BGLAP2 (12097)	Forward	AGACTCCGGCGCTACCTT	95 °C - 15 s; 60 °C - 30 s; 72 °C - 30 s
	Reverse	CTCGTCACAAGCAGGGTTAAG	
SPP1 (20750)	Forward	TTTGCTTTTGCCTGTTTGGC	95 °C - 15 s; 60 °C - 30 s; 72 °C - 30 s
	Reverse	CAGTCACTTTCACCGGGAGG	
DMP1 (13406)	Forward	CCCAAAACAGGAAAGGATCA	95 °C - 15 s; 60 °C - 30 s; 72 °C - 30 s
	Reverse	ACCAGACTGCTTCTCCTCCA	
GAPDH (14433)	Forward	AGGCCGGTGCTGAGTATGTC	95 °C - 15 s; 60 °C - 30 s; 72 °C - 30 s
	Reverse	TGCCTGCTTC ACCACCTTCT	

Quantitative PCR assay (qPCR). After being treated with conditioned medium by the different modified titanium surfaces for 24 h, the total mRNA of the cells was extracted using the Ambion TRIzol Reagent (Life Sciences - Fisher Scientific Inc, Walthan, MA, USA) and then these samples were treated with DNase I (Invitrogen, Carls-band, CA, USA). The synthesis of the cDNA was performed using a high capacity cDNA reverse transcription kit (Applied Biosystems, Foster City, CA, USA) based on the manufacturer's instructions. A 10 μl of sample containing PowerUp™SYBR™ Green Master Mix 2x (5 μl) (Applied Biosystems, Foster City, CA, USA), 0.4 μM of each primer, 50 ng of cDNA, and nuclease-free H_2O was performed using qPCR. The results were expressed as relative quantities of each selected target gene, using the Gapdh gene as housekeeping with the cycle threshold (Ct) method. The analyzed primers and their associated details are described in Table 1.

2.5. Statistical analysis

All the experiments were performed at least three times for better statistics, and the results were plotted as mean ± standard deviation (SD). A one-way analysis of variance (ANOVA) was performed using the Tukey test for multiple comparisons with the GraphPad Prism7 software (GraphPad Software Inc., San Diego, CA, USA) to evaluate whether different treated surfaces of the biomaterials influenced the adhesion or cell differentiation.

3. Results and discussion

In the last few decades, interest has increased about developing a biomaterial that can biologically interact with host tissue assembling
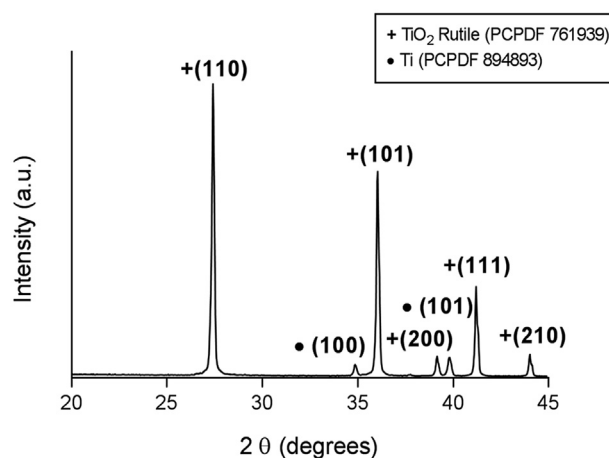

Figure 1. Crystallographic characterization of the rutile phase TiO_2 film.

properties of autogenous bone tissue, to improve osseointegration process and reduce implant failures. An important factor to consider is the surface properties, which are the first part of the implanted devices in contact with the host tissues and is expected to later drive cell behavior. To address this issue, we produced different modification on the titanium based surfaces and then performed *in vitro* tests to define the biological behavior of osteoblast cells responding to them, considering cell adhesion, ECM remodeling, and osteoblastic phenotype of these cells, which
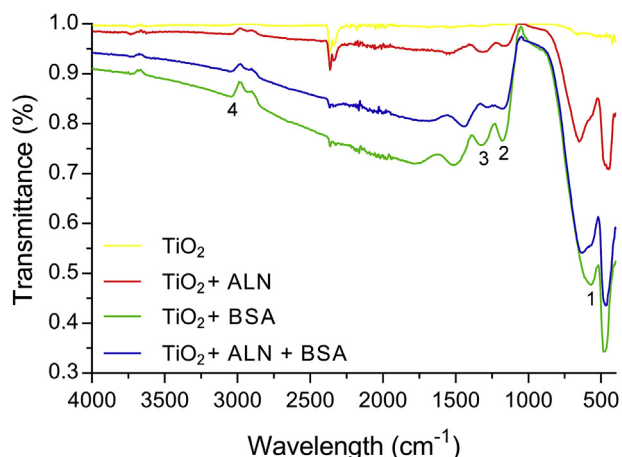
Figure 2. FTIR spectrum for alendronate (ALN) and albumin (BSA) functionalized samples.

are considered important outcomes to evaluate in response to titanium-based surfaces [5]. Considering the dynamism of the host biology in responding to implantable devices, we previously demonstrated that cells respond directly to the surfaces, but what about the indirect effects that trigger responses [8], especially considering neighboring cells.

Initially, the structural characterization of the TiO_2 thin films was performed using X-ray diffraction (XRD). The obtained XRD results indicate that the formed TiO_2 films had a rutile crystalline phase, as evidenced by the presence of a high-intensity diffraction peak (110) at 2θ = 27.4°, as shown in Figure 1.

Furthermore, Fourier transform infrared spectroscopy (FTIR) measurements confirm the effectiveness of the functionality, as shown in Figure 2. In the region between 570 and 648 cm^{-1} (1), observe the Ti–O bond band, relative to the TiO_2 film. The presence of P–O bonds is confirmed by bands in the region between 1160 and 1172 cm^{-1} (2), while values between 1279 and 1314 cm^{-1} (3) confirmed the existence of P=O bonds, in the alendronate molecule. The region between 3032 and 3045 cm^{-1} (4) refers to the binding of NH_2, which is present in both alendronate and albumin [33, 34, 35]. Thus, the functionalization of

rutile TiO_2 with alendronate and albumin was efficient, indicating that the prepared film was effectively functionalized.

X-ray photoelectron spectroscopy (XPS) experiments were performed to better analyze the chemical compositions of the surfaces and the electronic states of the functionalized materials. The spectrum of TiO_2 emphasizes the presence of the TiO_2 film due to the higher O 1s peak intensity (Figure 3a). The Ti $2p^1/_2$ (464.4 eV) and Ti $2p^3/_2$ (458.7 eV) contributions [36] (Figure 3b) are two peaks associated with the contributions from the base metal and have an energy difference of 5.7 eV, which is consistent with the oxidation state Ti^{+4} presented in TiO_2. The high-resolution spectrum for the O 1s peak (Figure 3c) is the convolution of three peaks. The two low energy peaks are related to the TiO_2 metal oxide bonds [37]. The third contribution has the highest energy and is related to the oxygen of the Ti–OH bond [36].

Figure 4a illustrates the presence of the O 1s, Ti 2p, N 1s, P 2p, and C 1s peaks for the alendronate functionalized surfaces (TiO_2 + ALN). The presence of the N 1s and P 2p peaks in the survey spectrum is related to the elemental nitrogen and phosphorous from the alendronate, validating the presence of this molecule at the surface. The high-resolution spectrum (Figure 4b to 4e) indicates the functionalization of the surfaces. The O 1s spectrum, in Figure 4b shows a peak at 532.0 eV associated with the P–O/OH [38], which is also related to the alendronate. The Ti–O peak with a binding energy of 530.0 eV indicates the presence of the oxide layer [39].

The three different contributions to the C 1s peak (Figure 4c) are at 285.3 eV (C–C), 286.7 eV (C–O/C–N) [40], and 289.3 eV (C-PO (OH)$_2$) [41]. The presence of the C-N and C-PO (OH)$_2$ bonds confirm the existence of alendronate on the surface. Finally, the N 1s spectrum (Figure 4d) confirms the functionalization due to the NH_3^+ [42] peak at 401.2 eV and the organic binding C–N at 399.2 eV [40]. The presence of NH_3^+ suggests that it could have been generated by the formation of a zwitterionic amine structure, which favors adsorption through the C-PO(OH)$_2$ group [43, 44]. Figure 4e shows the high-resolution spectrum for P 2p, which contains two contributions, P $2p^1/_2$ (134.5 eV) and P $2p^3/_2$ (133.3 eV) [36], confirming the presence of alendronate on the TiO_2 surface.

The evaluation of the albumin functionalized surfaces is presented in Figure 5. The TiO_2 + BSA survey spectrum (Figure 5a) demonstrates increased binding energy for the N 1s and C 1s signals compared to the
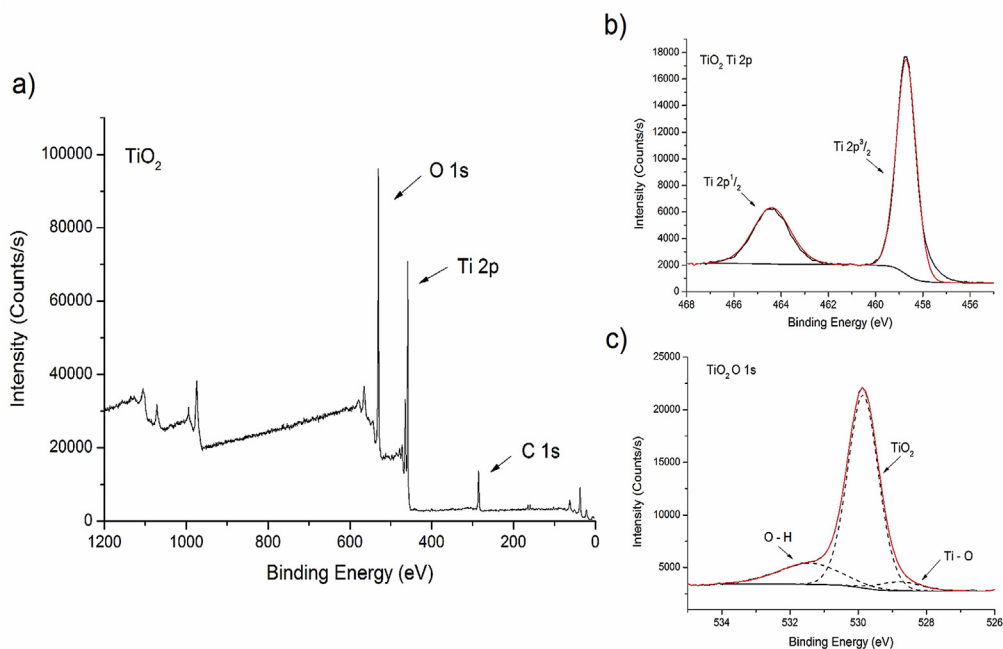

Figure 3. XPS survey spectrum of the TiO_2 (a), high-resolution Ti 2p spectrum (b), and high-resolution O 1s spectrum (c).
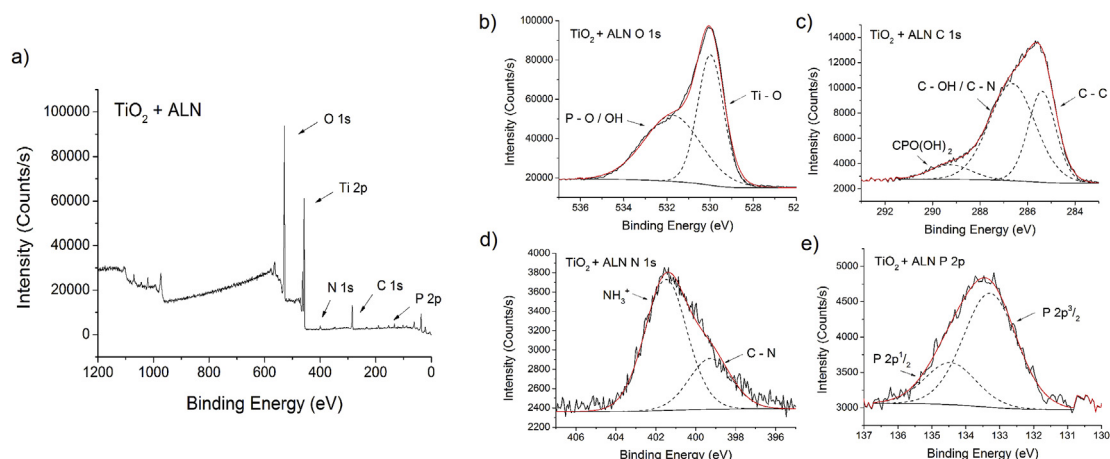
Figure 4. XPS survey spectrum of the TiO_2 + ALN (a), high-resolution O 1s spectrum (b), high-resolution C 1s spectrum (c), high-resolution N 1s spectrum (d), and high-resolution P 2p spectrum (e).
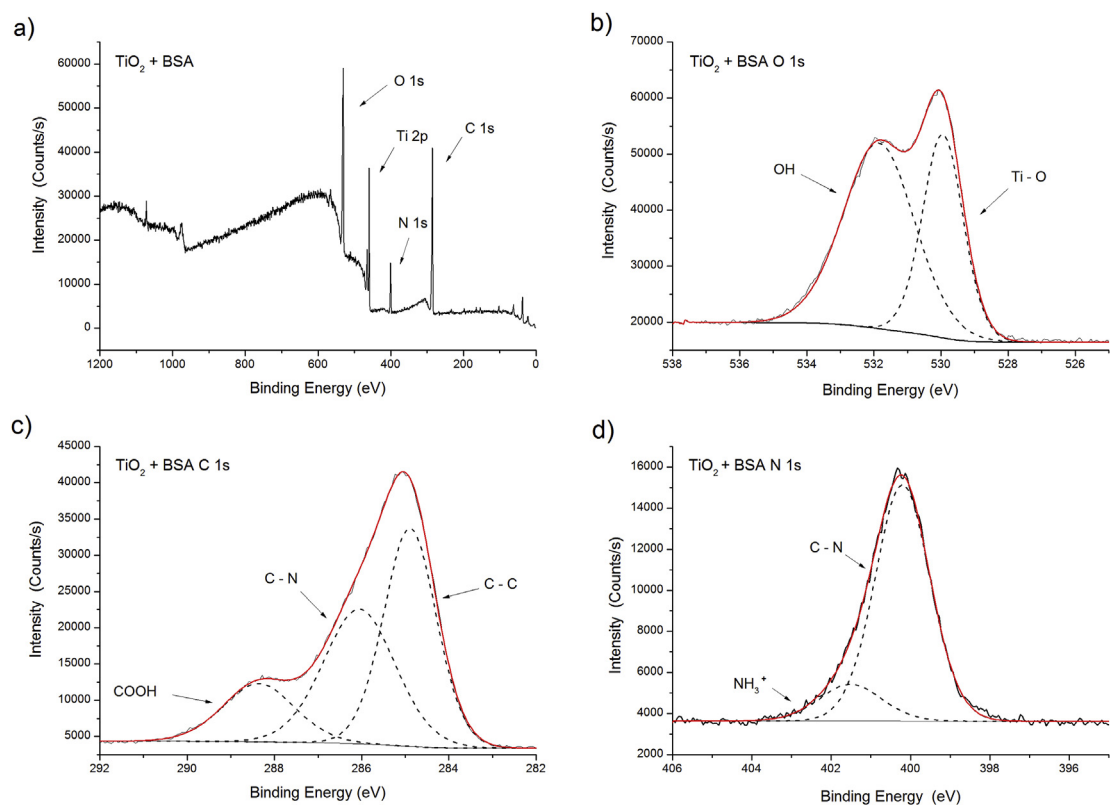

Figure 5. XPS survey spectrum of the TiO_2 + BSA (a), high-resolution O 1s spectrum (b), high-resolution C 1s spectrum (c), and high-resolution N 1s spectrum (d).

alendronate-functionalized surfaces, which may be due to the chemical composition of albumin. The O 1s spectrum in Figure 5b contains the OH (531.8 eV) and Ti–O (529.9 eV) [45] peaks for the titanium bonds. The three contributions present for the C 1s spectrum (Figure 5c) are all related to the albumin functionalization. The N 1s spectrum (Figure 5d) indicates that the peak at 401.5 eV [42] is related to the presence of NH_3^+ in the albumin molecule, as well as the high-intensity C–N peak.

Additionally, the TiO_2 + ALN + BSA survey spectrum in Figure 6a has peaks associated with the functionalization of the two compounds. In Figure 6b, the OH contributions (531.9 eV) and Ti–O (530.0 eV) peaks were nearly the same as the albumin-only functionalization. For the C 1s spectrum (Figure 6c), the three different contributions are the COOH/C-PO $(OH)_2$, C–N, and C–C. The presence of the COOH groups are due to the

albumin, while the C-PO $(OH)_2$ groups are from alendronate. In the N 1s spectrum (Figure 6d), contributions from the NH_3^+ (401.2 eV) and C–N (400.3 eV) [41] found may be related to the active functionalization of both alendronate and albumin. In Table 2, a compositional analysis of high-resolution XPS peaks is provided.

The surface roughness of the samples was investigated using Confocal Optical Microscopy considering the arithmetic surface roughness (Ra). Figures 7, 8, 9, 10, and 11 are 2D and 3D images obtained from the surface roughness analysis of the samples.

First, we verify whether the medium conditioned by the modified surfaces was cytotoxic, and the results showed a higher mitochondrial dehydrogenase activity in all modified groups, presenting more viable cells that the control (polished Ti), especially in TiO_2 + BSA (Figure 12a).

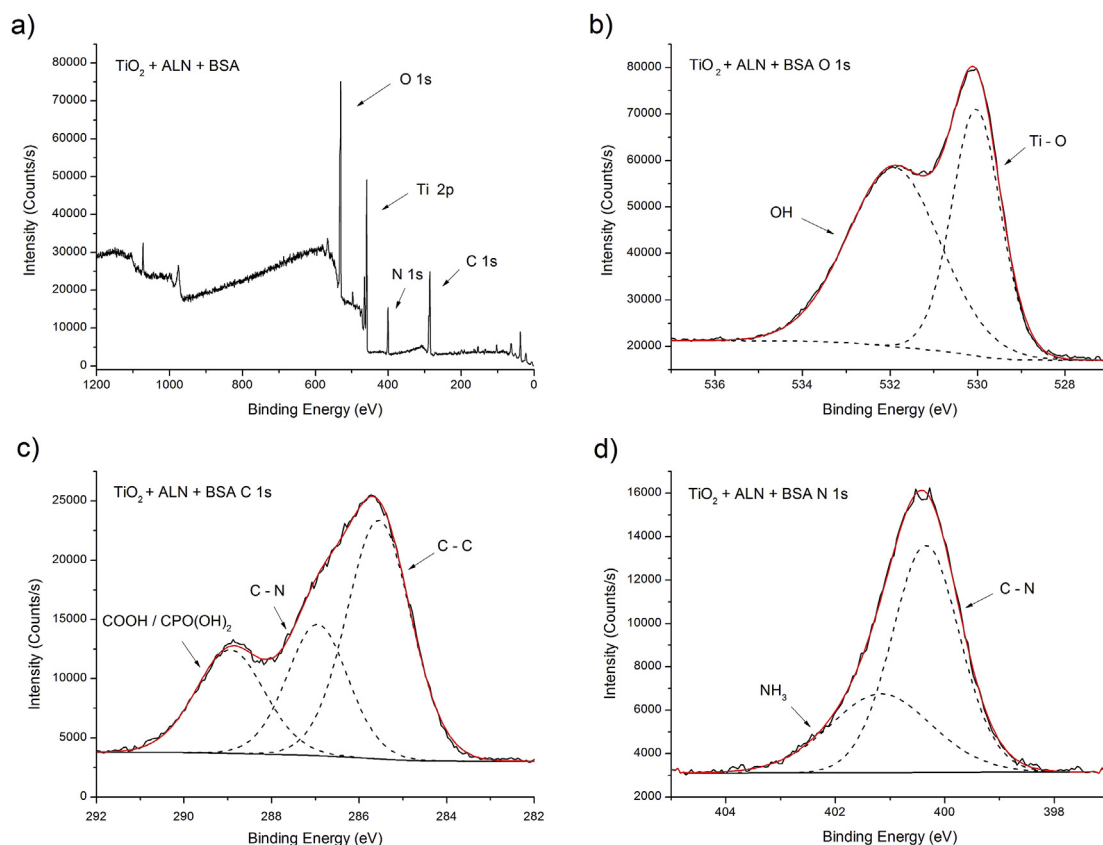**Figure 6.** XPS survey spectrum for the TiO$_2$ + ALN + BSA (a), high-resolution O 1s spectrum (b), high-resolution C 1s spectrum (c), and high-resolution N 1s spectrum (d).

Table 2. Compositional analysis of high resolution XPS peaks.

	TiO$_2$ (Figure 3)	TiO$_2$ + ALN (Figure 4)	TiO$_2$ + BSA (Figure 5)	TiO$_2$ + ALN + BSA (Figure 6)
Ti 2p				
O 1s	TiO$_2$ – 77.89% TiO – 5.02% O–H – 17.09%	OH/P–O – 52.71% Ti–O – 47.29%	OH – 61.52% Ti–O – 38.48%	OH – 58.12% Ti–O – 41.88%
C 1s		C–N – 33.13% C–OH – 58.92% C – 7.95%	C–C – 45.34% COOH – 16.50% C–N – 38.16%	C–N – 50.34% COOH – 23.41% C – 26.24%
N 1s		NH$_3$ – 72.09% C–N – 27.91%	C–N – 85.05% NH$_3$ – 14.95%	NH$_3$ – 34.30% N – 63.70%
P 2p		2p3/2–73.87% 2p1/2–26.13%		2p3/2–65.76% 2p1/2–26.35% Na$_3$PO$_4$ – 7.89%

After the non-toxicity of the conditioned medium by the surfaces was identified, the cell adhesion was evaluated using violet crystal and a standardization of the number of adhered cells was observed in all groups (Figure 12b). These results suggest a differential metabolic behavior of the osteoblast cells interacting with the different titanium surfaces evaluated in this study, which prompted us to better address the molecular behavior of these cells.

To better understand the intracellular mechanisms involved in adhesion events, we evaluated genes related to cell adhesion using qPCR technology. The results illustrate a repertory of genes related to cell adhesion. First, the gene expression of *Integrin-β1* (Figure 13a) was differently required considering the biomaterials, with a significant decrease in response to TiO$_2$ + ALN and an significant increase in response to TiO$_2$ + BSA and TiO$_2$ + ALN + BSA. *Integrin* has subunits (α and β) that are correlated with transduction of signals, connecting with

ECM proteins and other signaling proteins included in cell proliferation and migration processes [46]. Integrin activation benefits the interaction with other key proteins involved in this cellular signaling cascade, such as Fak and Src, responsible for cell-surface interaction, which exhibited significant gene expression on remodeled surfaces [47, 48]. Therefore, we investigated the behavior of both *Fak* and *Src* genes. Figures 13b and 13c show a panorama of the expression very similar to *Integrin-β1*. *Fak* and *Src* were probably activated before 24 h when in contact with the different surfaces; however, these results highlight that both these genes are modulated during the phenotype changes of these cells.

Cytoskeleton rearrangement is an important event during cell adhesion; therefore, we also investigated genes related with this condition and found that the expression of *Cofilin* significantly decreased in response to TiO$_2$ + ALN (Figure 13d). As *Cofilin* activity is modulated by phosphorylation at Ser, we evaluated Ser/Thr phosphatase. The activity of the
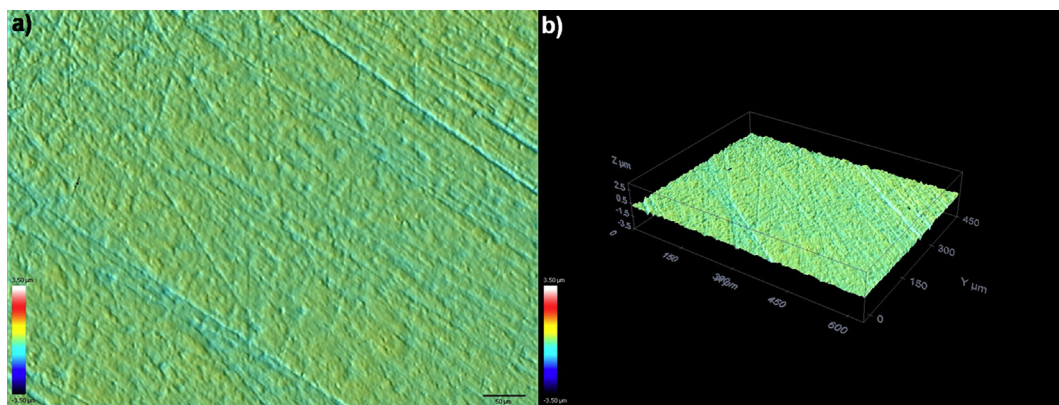
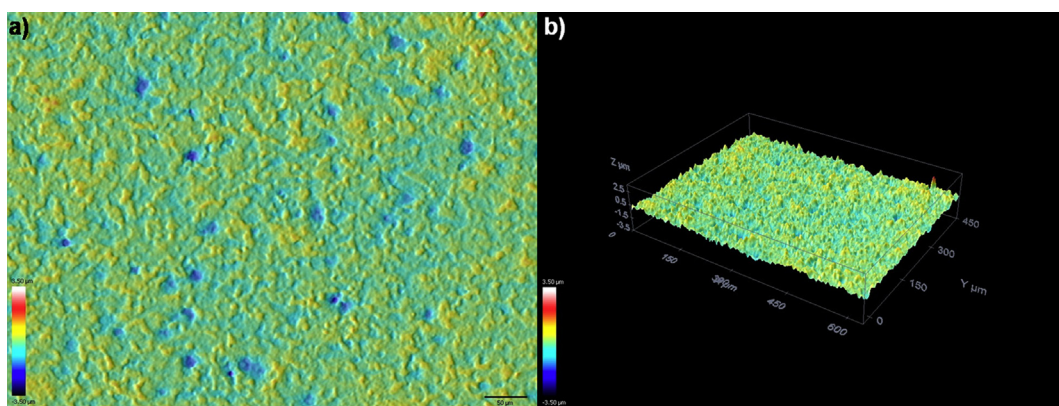**Figure 7.** Confocal Optical Microscopy image for the sanded Ti Cp4 sample in 2D (a) and 3D (b).

Figure 8. Confocal Optical Microscopy image for the sanded TiO_2 sample in 2D (a) and 3D (b).
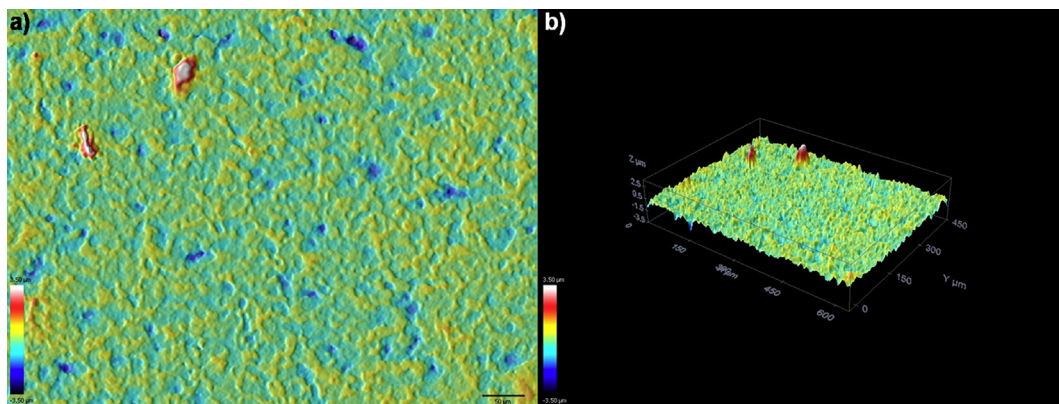

Figure 9. Confocal Optical Microscopy image for the sanded TiO_2 + ALN sample in 2D (a) and 3D (b).

Pp2A gene decreased in osteoblast responding to TiO_2 + ALN and TiO_2 + BSA (Figure 13e). The osteoblast clearly responded differently to the proposed surfaces, modifying their phenotype and requiring genes related to cell adhesion and cytoskeleton rearrangement. In addition, an important axis of intracellular signaling seems to require *Pp2A* to modulate the *Cofilin* activity through transient dephosphorylating the Ser03.

The metabolism, involved in these cells challenged with the different surface compositions, displayed an important dynamism in the phenotypic variations necessary for this adaptive process, significantly interfering in responsive cells indirectly, which indicates that this event is something dynamic in the peri-implant tissue (considering this material

in the host). For this cell adhesion, supramolecular platforms explain this performance of adhesion as previously reported through behaviors of the Fak and Src genes. The importance was also highlighted of Src in adhesion processes due to osteoblast differentiation promoting important control in osteogenesis; which reflects a biphasic function of this protein in biological events to control the biology of these cells.

This interaction with these surfaces appears to be decisive for the subsequent events of cellular performance and might even contribute to important biological events of matrix rearrangement through the activity of metalloproteinases (MMPs) [5, 7, 49, 50, 51]. Therefore, we evaluated ECM-related genes by considering the behavior of both gene and gelatinolytic activities of MMPs by zymography technology. We obtained
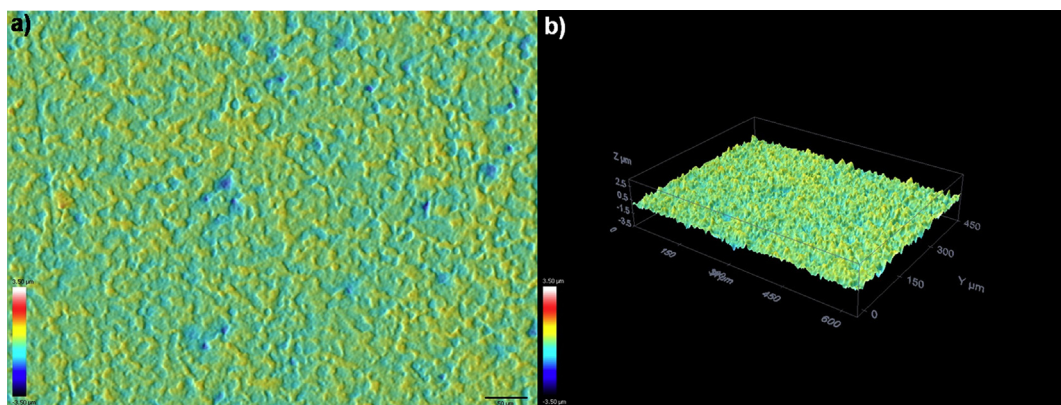
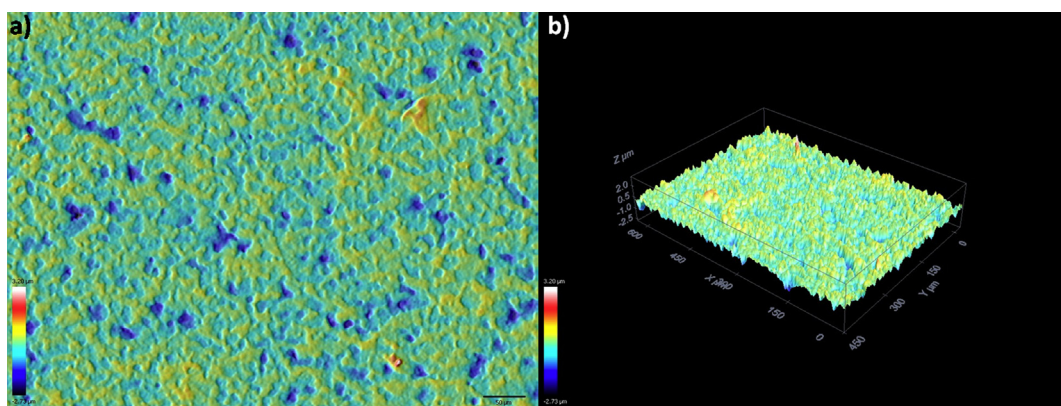**Figure 10.** Confocal Optical Microscopy image for the sanded TiO_2 + BSA sample in 2D (a) and 3D (b).

Figure 11. Confocal Optical Microscopy image for the sanded TiO_2 + ALN + BSA sample in 2D (a) and 3D (b).
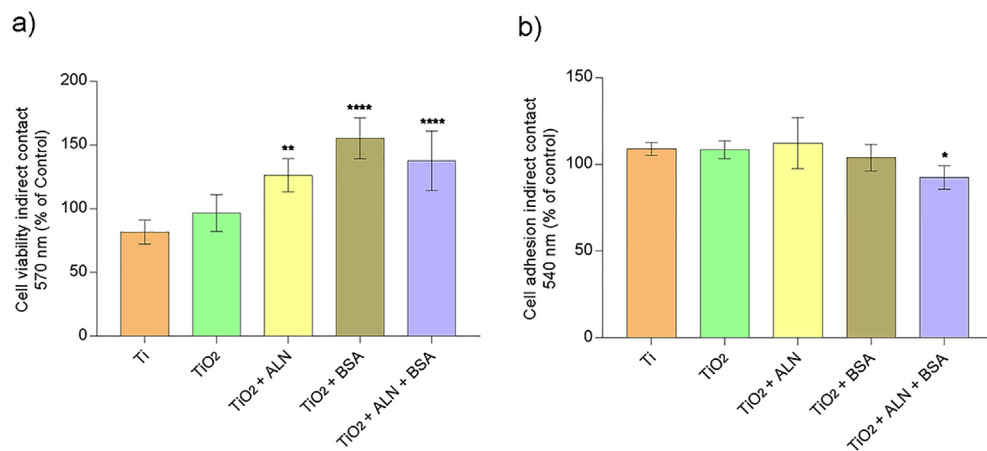

Figure 12. Cell survival and adhesion behavior promoted by the different surfaces. Cytotoxic effects of TiO_2-modified surfaces were measured by mitochondrial dehydrogenase activity (MTT assay) as represented by the percentage of cellular viability of the pre-osteoblasts (a). Cell adhesion was evaluated when pre-osteoblasts were treated up to 24 h with enriched medium from modified surfaces and the adherent cells were stained with violet crystals (b). A one-way ANOVA was performed with Tukey's test as a multiple comparison test to evaluate the effects of different treated surfaces on the cellular adhesion. The results are represented as the mean $\pm$ SD of three independent experiments. Differences were considered when * for $p < 0.05$, ** for $p < 0.001$, and **** for $p < 0.0001$.

significantly increased expression of *Timp2* gene (Figure 14a) in all modified groups, especially in TiO_2 + ALN + BSA; while the *Mmp2* gene (Figure 14b) decreased compared to the control (Ti). Figure 14c illustrates an over expression of *Mmp9* for all the modified surfaces, suggesting a balance between Mmp2 and Mmp9 in those conditions. The zymography assay for the activity of the MMPs indicated a significant increase of both MMPs activities in response to TiO_2 + ALN group (Figure 14d-j; Figure S1). We suggest that the dynamic ECM remodeling may be a prerequisite to late biomineralization events, where ECM rearrangement is necessary for the nucleation of hydroxyapatite, the major mineral constituent of bone.

The extracellular matrix (ECM) provides a scaffold for cells, mainly considering adhesion, proliferation, and differentiation, and their remodeling is described as a fundamental activity to improve these functions [52]. Matrix metalloproteinases (MMPs) are zinc endopeptidases responsible for the regulation of various mechanisms including the remodeling of the extracellular matrix rearrangement [53]. During osteoblastic differentiation, extracellular remodeling is strictly controlled through the balanced activity of MMPs and their tissue inhibitors, *Timps*, which were very dynamic in response to the surfaces. In particular, *Timp2* plays an important role in osteoblastic differentiation, and its expression positively modulates MMPS activity. The expression of *Mmp2* and *Mmp9*
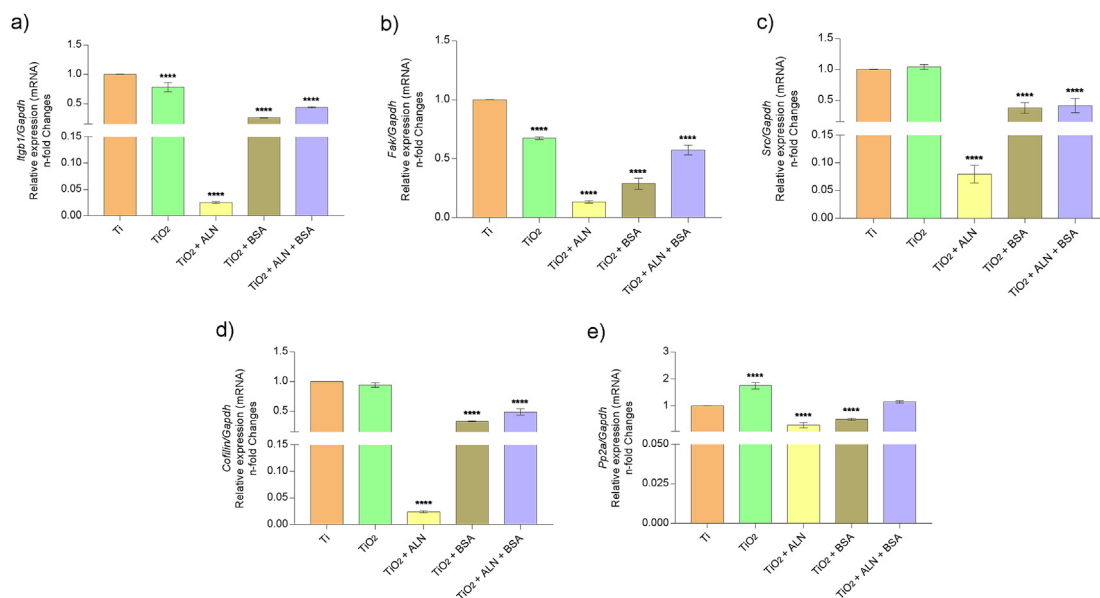
Figure 13. Differential behavior of osteoblast responding to different titanium-based surfaces – a special look at cell adhesion mechanism. The total mRNA was collected and adhesion-related genes (*Integrin*, *Fak*, *Src*, *Cofilin*, and *Pp2A*) evaluated by utilizing qPCR technology (a–e). The results are represented as the mean ± SD of three independent experiments. A one-way ANOVA was performed with Tukey's test as a multiple comparison test to evaluate the effects of different treated surfaces on the cellular adhesion. Differences were considered when * for $p < 0.05$, ** for $p < 0.001$, and **** for $p < 0.0001$.
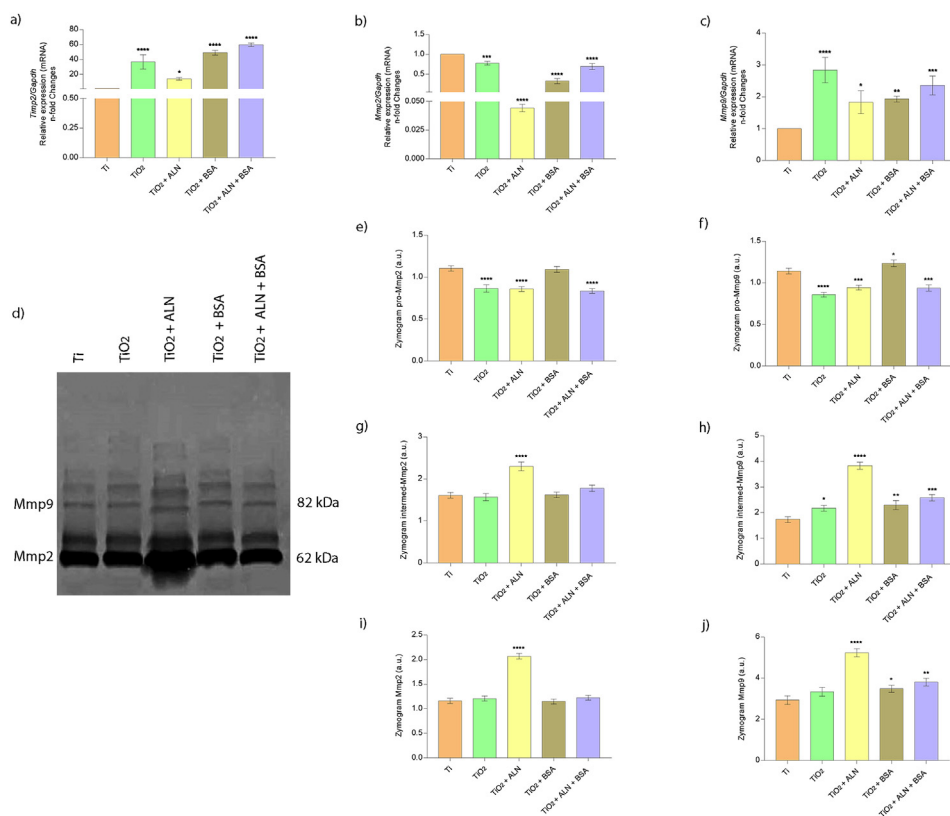

Figure 14. Extracellular matrix (ECM) remodeling after indirect contact with osteoblast responding to different biofunctionalized surfaces. The profile expression of the genes involved in the rearrangement of the extracellular matrix (ECM) - *Timp2* (a), *Mmp2* (b) and *Mmp9* (c) were analyzed using qPCR technology. In addition, MMP activities were measured by the zymography technology (d; Fig. S1) and the analysis of those activities of both *Mmp2* (e, g, i) and *Mmp9* (f, h, j) are shown. The results are represented as the mean ± standard deviation from three independent experiments. A one-way ANOVA was performed with Tukey's test as a multiple comparison to evaluate the effects of different treated surfaces in the extracellular matrix, where * for $p < 0.05$, ** for $p < 0.01$, *** for $p < 0.001$, and **** for $p < 0.0001$.

together with the enzymatic activity indicated remodeling of the ECM in the different modified surfaces, which was also demonstrated by another study [54].

Subsequently, the mineralizing phenotype of these cells was evaluated respecting the biomarker analysis of the osteoblastic differentiation, by examining the following genes: *Runx2*, Alkaline Phosphatase (*Alp*), Bone Sialoprotein (*Bsp*), Osteopontin (*Spp1*), Osteocalcin (*Bglap2*), and

the Dentin Matrix Protein (*Dmp1*) (Figure 15). Our results show that *Runx2* expression increased about 15-fold in response to TiO$_2$ + ALN compared to control (Figure 15a), suggesting a strong involvement of this treatment on osteoblastic phenotype. A similar behavior in response to TiO$_2$ + ALN (~3-fold change) was observed considering the *Alp* gene, which is an essential gene for bone mineralization events [55] (Figure 15b). The *Bsp* gene is related to the deposition of hydroxyapatite
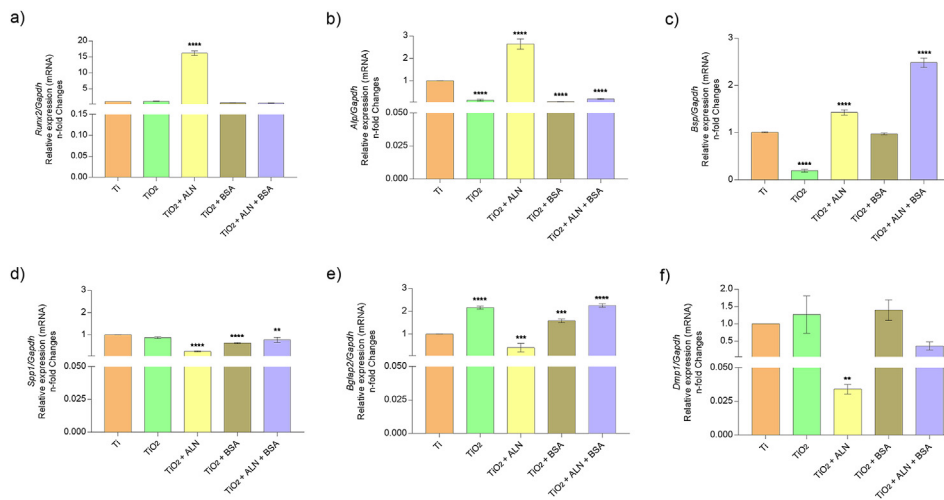
Figure 15. Biofunctionalized titanium surfaces differentially promote osteoblastic-related genes. The cells were harvested in TriZOL for RNA extraction and subsequent cDNA synthesis. The $Runx_2$ (a), Alp (b), Bsp(c), $Spp1$ (d), $Bglap2$ (e), and $DMP1$ (f) genes were each analyzed, and the results are represented as the mean $\pm$ standard deviation of three independent experiments. A one-way ANOVA was performed with Tukey's test as a multiple comparison to evaluate the effects of different treated surfaces on the genes related to the process and regulation of osteoblastic differentiation, where ** for $p < 0.01$, ***, and **** for $p < 0.0001$.

in the bone matrix, and its expression significantly increased on the surfaces of TiO_2 + ALN and TiO_2 + ALN + BSA (Figure 15c). Other genes were found to be involved with in this process such as $Spp1$ (Figure 15d) and $Bglap2$ (Figure 15e). The expression of $Dmp1$, which is responsible for the maturation of osteoblasts [56], decreased in response to TiO_2 + ALN considering this biological model (Figure 15f).

4. Conclusion

Finally, despite the limitations of an in vitro study and the short time of cell-surface interaction considered in this study, we observed interesting osteogenic behavior on alendronate and albumin surfaces. Now in vivo analyses in needed to better consider these surfaces for clinical trials within biomedical area.

Declarations

Author contribution statement

Carolina S. Albano: Conceived and designed the experiments; Performed the experiments; Analyzed and interpreted the data; Wrote the paper.

Anderson M. Gomes, Geórgia da Silva Feltran, Célio Junior da Costa Fernandes: Performed the experiments; Wrote the paper.

Luciana Daniele Trino: Performed the experiments; Analyzed and interpreted the data; Wrote the paper.

Willian Fernando Zambuzzi, Paulo Noronha Lisboa-Filho: Conceived and designed the experiments; Analyzed and interpreted the data; Contributed reagents, materials, analysis tools or data; Wrote the paper.

Funding statement

Competing interest statement

The authors declare no conflict of interest.

Additional information

Supplementary content related to this article has been published online at https://doi.org/10.1016/j.heliyon.2020.e04455.

References

[1] E. Mariani, G. Lisignoli, R.M. Borzì, L. Pulsatelli, Biomaterials: foreign bodies or tuners for the immune response? Int. J. Mol. Sci. 20 (2019).

[2] K.V. Smyrnova, A.D. Pogrebnjak, L.G. Kassenova, Structural features and properties of biocompatible Ti-based alloys with β-stabilizing elements, in: A. Pogrebnjak, V. Novosad (Eds.), Advances in Thin Films, Nanostructured Materials, and Coatings. Lecture Notes in Mechanical Engineering, Springer, Singapore, 2019.

[3] Q. Chen, G.A. Thouas, Metallic implant biomaterials, Mater. Sci. Eng. R Rep. 87 (2015) 1–57.

[4] G. da S. Feltran, F. Bezerra, C.J. da Costa Fernandes, M.R. Ferreira, W.F. Zambuzzi, Differential inflammatory landscape stimulus during titanium surfaces obtained osteogenic phenotype, J. Biomed. Mater. Res. 107 (2019) jbm.a.36673.

[5] C.J. da Costa Fernandes, F.J.B. Bezerra, B. de Campos Souza, M.A. Campos, W.F. Zambuzzi, Titanium-enriched medium drives low profile of ECM remodeling as a pre-requisite to pre-osteoblast viability and proliferative phenotype, J. Trace Elem. Med. Biol. 50 (2018) 339–346.

[6] M. Baroncelli, G.M. Fuhler, J. Peppel, W.F. Zambuzzi, J.P. Leeuwen, B.C.J. Eerden, M.P. Peppelenbosch, Human mesenchymal stromal cells in adhesion to cell derived extracellular matrix and titanium: comparative kinome profile analysis, J. Cell. Physiol. 234 (2019) 2984–2996.

[7] C.J.C. Fernandes, F. Bezerra, M.R. Ferreira, A.F.C. Andrade, T.S. Pinto, W.F. Zambuzzi, Nano hydroxyapatite-blasted titanium surface creates a biointerface able to govern Src-dependent osteoblast metabolism as prerequisite to ECM remodeling, Colloids Surf. B Biointerfaces 163 (2018) 321–328.

[8] M.C. Rossi, F.J.B. Bezerra, R.A. Silva, B.P. Crulhas, C.J.C. Fernandes, A.S. Nascimento, V.A. Pedrosa, P. Padilha, W.F. Zambuzzi, Titanium-released from dental implant enhances pre-osteoblast adhesion by ROS modulating crucial intracellular pathways, J. Biomed. Mater. Res. 105 (2017) 2968–2976.

[9] M. Catauro, F. Bollino, F. Papale, Biocompatibility improvement of titanium implants by coating with hybrid materials synthesized by sol-gel technique, J. Biomed. Mater. Res. 102 (2014) n/a-n/a.

[10] M. Abdel-Hady Gepreel, M. Niinomi, Biocompatibility of Ti-alloys for long-term implantation, J. Mech. Behav. Biomed. Mater. 20 (2013) 407–415.

[11] X. Liu, P.K. Chu, C. Ding, Surface modification of titanium, titanium alloys, and related materials for biomedical applications, Mater. Sci. Eng. R Rep. 47 (2004) 49–121.

[12] J.M. Morais, F. Papadimitrakopoulos, D.J. Burgess, Biomaterials/tissue interactions: possible solutions to overcome foreign body response, AAPS J. 12 (2010) 188–196.

[13] A. Ochsenbein, F. Chai, S. Winter, M. Traisnel, J. Breme, H.F. Hildebrand, Osteoblast responses to different oxide coatings produced by the sol–gel process on titanium substrates, Acta Biomater. 4 (2008) 1506–1517.

[14] S.A. Alves, R. Bayón, V.S. de Viteri, M.P. Garcia, A. Igartua, M.H. Fernandes, L.A. Rocha, Tribocorrosion behavior of calcium- and phosphorous-enriched titanium oxide films and study of osteoblast interactions for dental implants, J. Bio-Tribo-Corrosion. 1 (2015) 23.

[15] M.B. Guimarães, T.H. Antes, M.B. Dolacio, D.D. Pereira, M. Marquezan, Does local delivery of bisphosphonates influence the osseointegration of titanium implants? A systematic review, Int. J. Oral Maxillofac. Surg. 46 (2017) 1429–1436.

[16] J. Abtahi, P. Tengvall, P. Aspenberg, A bisphosphonate-coating improves the fixation of metal implants in human bone. A randomized trial of dental implants, Bone 50 (2012) 1148–1151.

[17] P. Tengvall, B. Skoglund, A. Askendal, P. Aspenberg, Surface immobilized bisphosphonate improves stainless-steel screw fixation in rats, Biomaterials 25 (2004) 2133–2138.

[18] J. Abtahi, P. Tengvall, P. Aspenberg, Bisphosphonate coating might improve fixation of dental implants in the maxilla: a pilot study, Int. J. Oral Maxillofac. Surg. 39 (2010) 673–677.

[19] A. Carano, S.L. Teitelbaum, J.D. Konsek, P.H. Schlesinger, H.C. Blair, Bisphosphonates directly inhibit the bone resorption activity of isolated avian osteoclasts in vitro, J. Clin. Invest. 85 (1990) 456–461.

[20] K. Wermelin, P. Aspenberg, P. Linderbäck, P. Tengvall, Bisphosphonate coating on titanium screws increases mechanical fixation in rat tibia after two weeks, J. Biomed. Mater. Res. 86A (2008) 220–227.

[21] K. Wermelin, F. Suska, P. Tengvall, P. Thomsen, P. Aspenberg, Stainless steel screws coated with bisphosphonates gave stronger fixation and more surrounding bone. Histomorphometry in rats, Bone 42 (2008) 365–371.

[22] M. Talha, Y. Ma, P. Kumar, Y. Lin, A. Singh, Role of protein adsorption in the bio corrosion of metallic implants – a review, Colloids Surf. B Biointerfaces 176 (2019) 494–506.

[23] E. Anbazhagan, A. Rajendran, D. Natarajan, M.S. Kiran, D.K. Pattanayak, Divalent ion encapsulated nano titania on Ti metal as a bioactive surface with enhanced protein adsorption, Colloids Surf. B Biointerfaces 143 (2016) 213–223.

[24] M. Kawashita, J. Hayashi, Z. Li, T. Miyazaki, M. Hashimoto, H. Hihara, H. Kanetaka, Adsorption characteristics of bovine serum albumin on to alumina with a specific crystalline structure, J. Mater. Sci. Mater. Med. 25 (2014) 453–459.

[25] J. Hayashi, M. Kawashita, T. Miyazaki, M. Kamitakahara, K. Ioku, H. Kanetaka, Comparison of Adsorption Behavior of Bovine Serum Albumin and Osteopontin on Hydroxyapatite and Alumina, 2012. https://www.jstage.jst.go.jp/article/prb/26/0/26_23/_pdf/-char/en. (Accessed 17 July 2019).

[26] L.D. Trino, E.S. Bronze-Uhle, A. Ramachandran, P.N. Lisboa-Filho, M.T. Mathew, A. George, Titanium surface bio-functionalization using osteogenic peptides: surface chemistry, biocompatibility, corrosion and tribocorrosion aspects, J. Mech. Behav. Biomed. Mater. 81 (2018) 26–38.

[27] D. Zheng, K.G. Neoh, E.-T. Kang, Immobilization of alendronate on titanium via its different functional groups and the subsequent effects on cell functions, J. Colloid Interface Sci. 487 (2017) 1–11.

[28] M.C.L. Martins, B.D. Ratner, M.A. Barbosa, Protein adsorption on mixtures of hydroxyl- and methyl-terminated alkanethiols self-assembled monolayers, J. Biomed. Mater. Res. 67A (2003) 158–171.

[29] L.D. Trino, E.S. Bronze-Uhle, A. George, M.T. Mathew, P.N. Lisboa-Filho, Surface physicochemical and structural analysis of functionalized titanium dioxide films, Colloid. Surface. Physicochem. Eng. Aspect. 546 (2018) 168–178.

[30] T. Mosmann, Rapid colorimetric assay for cellular growth and survival: application to proliferation and cytotoxicity assays, J. Immunol. Methods 65 (1983) 55–63. http://www.ncbi.nlm.nih.gov/pubmed/6606682. (Accessed 14 February 2019).

[31] O.H. Lowry, N.J. Rosebrough, A.L. Farr, R.J. Randall, Protein measurement with the Folin phenol reagent, J. Biol. Chem. 193 (1951) 265–275. http://www.ncbi.nlm.nih.gov/pubmed/14907713. (Accessed 24 July 2018).

[32] V. Lefebvre, C. Peeters-Joris, G. Vaes, Production of gelatin-degrading matrix metalloproteinases ('type IV collagenases') and inhibitors by articular chondrocytes during their dedifferentiation by serial subcultures and under stimulation by interleukin-1 and tumor necrosis factor α, Biochim. Biophys. Acta Mol. Cell Res. 1094 (1991) 8–18.

[33] X. Liu, Preparation and characterization of pure anatase nanocrystals by sol-gel method, Powder Technol. 224 (2012) 287–290.

[34] X. Liu, S. Qu, X. Lu, X. Ge, Y. Leng, Time-of-flight secondary ion mass spectrometry study on the distribution of alendronate sodium in drug-loaded ultra-high molecular weight polyethylene, Biomed, Mater. 4 (2009).

[35] P.D.L.H. Madkour, A Handbook of Spectroscopic Data CHEMISTRY (UV, JR, PMR, JJCNMR and Mass Spectroscopy), Oxford Book Company, Jaipur, India, 2009.

[36] J.F. Moulder, W.F. Stickle, P.E. ' Sobol, K.D. Bomben, J. Chastain, Handbook of X-ray Photoelectron Spectroscopy AReference Book of Standard Spectra for Identification and Interpretation of XPS Data, 2000 n.d.https://www.cnyn.unam.mx/~wencel/XPS/MANXPS.pdf. (Accessed 25 July 2018).

[37] M. Shahnas Beegam, S.B. Narendranath, P. Periyat, Tuning of selective solar photocatalysis by Mn^{2+} decorated nanocrystalline mesoporous TiO_2, Sol. Energy 158 (2017) 774–781.

[38] H. Zhang, H. Jiang, Y. Hu, H. Jiang, C. Li, Integrated Ni-P-S nanosheets array as superior electrocatalysts for hydrogen generation, Green Energy Environ. 2 (2017) 112–118.

[39] R. Narayan, P. Colombo, M. Halbig, S. Mathur, American Ceramic Society, Advances in Bioceramics and Porous Ceramics V: a Collection of Papers Presented at the 36th International Conference on Advanced Ceramics and Composites, John Wiley & Sons, Daytona Beach, Florida, January , 2013.

[40] J. Seop Lee, D. Hoon Shin, J. Jang, Electronic Supplementary Information (ESI) for Polypyrrole-Coated Manganese Dioxide with Multiscale Architectures for Ultrahigh Capacity Energy Storage, 2015. http://www.rsc.org/suppdata/c5/ee/c5ee02076j/c5ee02076j1.pdf. (Accessed 25 July 2018).

[41] S. Kačiulis, G. Mattogno, A. Napoli, E. Bemporad, F. Ferrari, A. Montenero, G. Gnappi, Surface analysis of biocompatible coatings on titanium, J. Electron. Spectrosc. Relat. Phenom. 95 (1998) 61–69.

[42] H. Hunke, N. Soin, T. Shah, E. Kramer, A. Pascual, M. Karuna, E. Siores, Low-pressure H_2, NH_3 microwave plasma treatment of polytetrafluoroethylene (PTFE) powders: chemical, thermal and wettability analysis, Materials 8 (2015) 2258–2275.

[43] E. Ataman, C. Isvoranu, J. Knudsen, K. Schulte, J.N. Andersen, J. Schnadt, Adsorption of L-cysteine on rutile TiO_2 (110), Surf. Sci. 605 (2011) 179–186.

[44] R. Nechikkattu, S.S. Park, C.-S. Ha, Zwitterionic functionalised mesoporous silica nanoparticles for alendronate release, Microporous Mesoporous Mater. 279 (2019) 117–127.

[45] X. Wang, S. Zhang, H. Wang, H. Yu, H. Wang, S. Zhang, F. Peng, Visible light photoelectrochemical properties of a hydrogenated TiO_2 nanorod film and its application in the detection of chemical oxygen demand, RSC Adv. 5 (2015) 76315–76320.

[46] H.T. Aiyelabegan, E. Sadroddiny, Fundamentals of protein and cell interactions in biomaterials, Biomed. Pharmacother. 88 (2017) 956–970.

[47] S.K. Mitra, D.D. Schlaepfer, Integrin-regulated FAK–Src signaling in normal and cancer cells, Curr. Opin. Cell Biol. 18 (2006) 516–523.

[48] F. Bezerra, M.R. Ferreira, G.N. Fontes, C.J. da Costa Fernandes, D.C. Andia, N.C. Cruz, R.A. da Silva, W.F. Zambuzzi, Nano hydroxyapatite-blasted titanium surface affects pre-osteoblast morphology by modulating critical intracellular pathways, Biotechnol. Bioeng. 114 (2017) 1888–1898.

[49] C.J. da Costa Fernandes, M.R. Ferreira, F.J.B. Bezerra, W.F. Zambuzzi, Zirconia stimulates ECM-remodeling as a prerequisite to pre-osteoblast adhesion/proliferation by possible interference with cellular anchorage, J. Mater. Sci. Mater. Med. 29 (2018) 41.

[50] T. Accorsi-Mendonça, W.F. Zambuzzi, K.B. da S. Paiva, J.R.P. Lauris, T.M. Cestari, R. Taga, J.M. Granjeiro, Expression of metalloproteinase 2 in the cell response to porous demineralized bovine bone matrix, J. Mol. Histol. 36 (2005) 311–316.

[51] W.F. Zambuzzi, K.B.S. Paiva, R. Menezes, R.C. Oliveira, R. Taga, J.M. Granjeiro, MMP-9 and CD68+ cells are required for tissue remodeling in response to natural hydroxyapatite, J. Mol. Histol. 40 (2009) 301–309.

[52] A.P. Liu, O. Chaudhuri, S.H. Parekh, New advances in probing cell-extracellular matrix interactions, Integr. Biol. (Camb). 9 (2017) 383–405.

[53] A. Mizutani, I. Sugiyama, E. Kuno, S. Matsunaga, N. Tsukagoshi, Expression of matrix metalloproteinases during ascorbate-induced differentiation of osteoblastic MC3T3-E1 cells, J. Bone Miner. Res. 16 (2001) 2043–2049.

[54] W.F. Zambuzzi, C.L. Yano, A.D.M. Cavagis, M.P. Peppelenbosch, J.M. Granjeiro, C.V. Ferreira, Ascorbate-induced osteoblast differentiation recruits distinct MMP-inhibitors: RECK and TIMP-2, Mol. Cell. Biochem. 322 (2009) 143–150.

[55] W.F. Zambuzzi, E.A. Bonfante, R. Jimbo, M. Hayashi, M. Andersson, G. Alves, E.R. Takamori, P.J. Beltrão, P.G. Coelho, J.M. Granjeiro, Nanometer scale titanium surface texturing are detected by signaling pathways involving transient FAK and Src activations, PloS One 9 (2014), e95662.

[56] A. George, E. Guirado, Y. Chen, DMP1 binds specifically to type I collagen and regulates mineral nucleation and growth, in: Biomineralization, Springer Singapore, Singapore, 2018, pp. 137–145.